Available online at www.sciencedirect.com

SciVerse ScienceDirect

Ceramics International 39 (2013) 7845–7851

CERAMICS INTERNATIONAL

www.elsevier.com/locate/ceramint

Dielectric, ferroelectric, magnetic and magnetoelectric properties of $0.1Ni_{0.8}Zn_{0.2}Fe_2O_4$–$0.9Pb_{1-3x/2}Sm_xZr_{0.65}Ti_{0.35}O_3$ magnetoelectric composites

Rekha Rani[a,d], J.K. Juneja[b,*], Sangeeta Singh[c], K.K. Raina[d], Chandra Prakash[e]

[a]*Electroceramics Research Laboratory, GVM Girls College, Sonepat 131001, India*
[b]*Department of Physics, Hindu College, Sonepat 131001, India*
[c]*Department of Physics, GVM Girls College, Sonepat 131001, India*
[d]*School of Physics & Materials Science, Thapar University, Patiala 147004, India*
[e]*Solid State Physics Laboratory, Timarpur, Delhi 110054, India*

Received 15 February 2013; received in revised form 22 February 2013; accepted 14 March 2013
Available online 21 March 2013

Abstract

Composites having general formula $0.1Ni_{0.8}Zn_{0.2}Fe_2O_4$–$0.9Pb_{1-3x/2}Sm_xZr_{0.65}Ti_{0.35}O_3$ with $x=0$, 0.01, 0.02 and 0.03 were synthesized by a conventional solid state reaction route. X-ray diffraction analysis was carried out to confirm the coexistence of individual phases and microstructural study was done by using a scanning electron microscope. Dielectric properties were studied as a function of temperature and frequency. To study ferroelectric and magnetic ordering in composite samples, *P–E* and *M–H* hysteresis loops were recorded respectively. Maximum magnetoelectric coupling coefficient of 22.5 mV/cm Oe was observed for sample with $x=0.03$. A significant improvement in dielectric, ferroelectric, piezoelectric and magnetoelectric properties was observed for Sm substitution.

Keywords: A. Sintering; C. Dielectric properties; C. Ferroelectric properties; D. PZT

1. Introduction

The study of magnetoelectric (ME) composites is one of the most popular area in the field of material science and it offers new ideas for multifunctional materials suitable for a variety of device applications like magnetic field sensors, multiple state memory elements, transducers, electro-optic devices, magnetically tuned capacitors, etc. [1–4]. In recent years, a combination of ferrites and ferroelectric materials has been extensively studied resulting in magnetostriction induced deformation (ferrite phase) and the generation of piezoelectric charge (ferroelectric phase). However, use of magnetoelectric composites for multifunctional device applications is still limited and various research groups have been trying to improve magnetoelectric coupling by suitable substitutions and better control of processing parameters. After literature survey, it has been observed that the studied systems correspond to substituted $NiFe_2O_4$, $CoFe_2O_4$, $MnFe_2O_4$, $CuFe_2O_4$, $ZnFe_2O_4$ with substituted PZT, PMN-PT, $BaTiO_3$, etc. [5].

For the present work, $Ni_{0.8}Zn_{0.2}Fe_2O_4$ (NZF) is chosen as ferrite phase having high electrical resistivity, low eddy current losses and high saturation magnetization [6,7]. Lead zirconate titanate (PZT) is chosen as ferroelectric phase because it has stronger dielectric and ferroelectric properties, higher electromechanical coupling coefficients, higher resistivity, higher Curie temperatures, lower sintering temperatures and is easier to pole as compared to $BaTiO_3$ [8–10]. It has been found that La^{+3} and Sm^{+3} (off-valent donors) substitution in PZT counteracts its p-type conductivity and increases its electrical resistivity. These substituents results in high dielectric constant, enhanced coupling factor, high remanant polarization and square hysteresis loop [11–13]. Thus addition of La and Sm to PZT phase is expected to give rise to improved magnetoelectric properties. Results of composites of nickel zinc ferrite and La substituted lead zirconate titanate (NZF–PLZT) has already been reported [14]. Here we are reporting the study on

*Corresponding author. Tel.: +91 9416260242.
E-mail address: jk_juneja@yahoo.com (J.K. Juneja).

0272-8842/$ - see front matter © 2013 Elsevier Ltd and Techna Group S.r.l. All rights reserved.
http://dx.doi.org/10.1016/j.ceramint.2013.03.045

composites of nickel zinc ferrite and Sm substituted lead zirconate titanate having general formula $0.1Ni_{0.8}Zn_{0.2}Fe_2O_4$–$0.9Pb_{1-3x/2}Sm_xZr_{0.65}Ti_{0.35}O_3$ (NZF–PSZT) with $x=0$, 0.01, 0.02 and 0.03.

2. Experimental

2.1. Material synthesis

The system containing two individual phases (NZF and PSZT) was synthesized by the conventional solid state reaction route which has already been described [14].

2.2. Characterization

Experimental density of the samples was determined using Archimede's principle. X-ray density of the samples was calculated using the lattice parameters. X-ray diffraction (XRD) data was recorded using a Philips XPERT-PRO Diffractogram with Cu-K_α ($\lambda=1.5406$ Å). Scanning electron microscope (SEM) micrographs of sintered samples were obtained using JEOL JSM 6510LV, Japan. For measuring electrical properties, the sintered pellets were grounded, lapped and then electroded properly using silver epoxy on flat surfaces and subsequent heating at 400 °C for 30 min. The dielectric properties were measured using an Agilent 4263B LCR meter. *P–E* hysteresis loops were recorded at 20 Hz using an automated *P–E* loop tracer based on the Sawyer–Tower circuit.

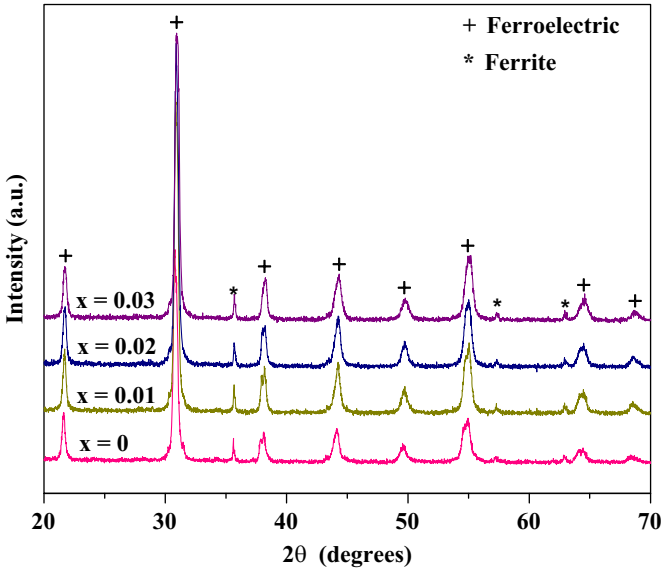

Fig. 1. XRD patterns for NZF–PSZT samples at room temperature.

For electric poling, samples were heated to 150 °C and a DC electric field (~15 kV/cm) was applied for 1 h. Then the samples were cooled to room temperature in the presence of field. *M–H* loops were recorded using a Lake Shore 735 VSM Controller, Model 662 interfaced with a computer. The magnetoelectric signal (voltage) was determined as a function of increasing DC magnetic field (0–2000 Oe) using 7265 DSP lock-in amplifier in the presence of small AC magnetic field ($H_{AC}=10$ Oe at 1 kHz). ME coupling coefficient, α was determined from the magnetoelectric signal (δV) using the formula [15]:

$$\alpha = \frac{\delta V}{tH_{AC}} \quad (1)$$

where δV is the magnetoelectric signal (voltage generated by applying magnetic field), t is the thickness of the sample and H_{AC} is the AC magnetic field.

3. Results and discussion

3.1. Structural properties

Fig. 1 shows the room temperature XRD patterns for NZF–PSZT samples. The analysis shows that all samples are polycrystalline, composed by mixtures of cubic spinel NZF phase and rhombohedral perovskite PSZT phase and no extra peak other than diffraction peaks corresponding to pure phases (NZF and PSZT) was found which indicate that no chemical reaction had occurred between the constituent phases during sintering of NZF–PSZT composites.

The ionic radius of Sm^{+3} (138 pm) is smaller than that of Pb^{+2} (163 pm), hence slight shifting in diffraction peaks corresponding to PSZT phase towards higher angle side is observed for higher Sm content. This indicates the slight decrease in lattice constant corresponding to PSZT phase as shown in Table 1. The variation in the values of lattice constant corresponding to NZF phase may be due to stress induced by a non-ferrite phase (PSZT) [16]. The experimental density, X-ray density and relative density values were determined for all samples and are given in Table 1. Such variations in density value are already observed for NZF–PLZT samples [14].

The SEM micrographs of the freshly broken surfaces for samples with $x=0.01$ and 0.03 are shown in Fig. 2. The micrographs show closely packed and well oriented grains. The shape, size and distribution of grains confirm the polycrystalline nature. Individual phases (NZF and PSZT) cannot

Table 1
Structural parameters for NZF–PSZT samples.

x	0	0.01	0.02	0.03
Lattice constant (Å) (NZF phase)	8.35	8.34	8.34	8.33
Lattice constant (Å) (PSZT phase)	4.10	4.10	4.09	4.09
Exp. density (g/cc)	6.88	6.91	6.89	7.04
X-ray density (g/cc)	7.75	7.72	7.71	7.69
Relative density (%)	88.8	88.2	89.4	91.5

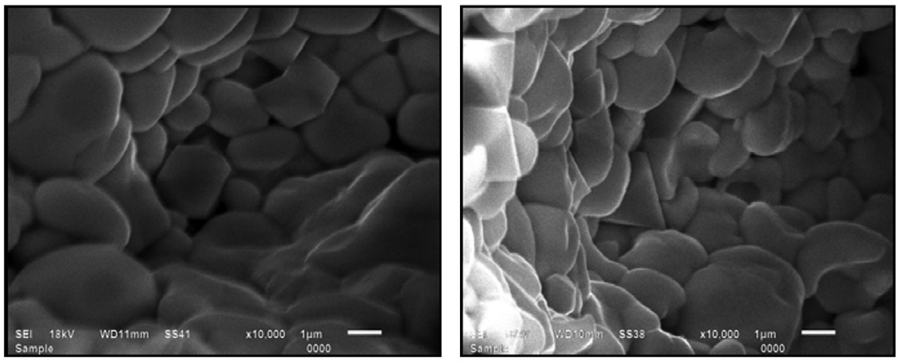

Fig. 2. SEM micrographs for NZF–PSZT samples with $x=0.01$ and 0.03.

be distinguished in SEM micrographs because of the small concentration of NZF phase.

3.2. Dielectric properties

The temperature variation of dielectric constant (ε') and loss ($\tan\delta$) at three selected frequencies (1, 10 and 100 kHz) is shown in Fig. 3. For all samples, as temperature increases, value of dielectric constant increases, attains a maximum at certain temperature (ferroelectric–paraelectric transition in PSZT phase) and then decreases with further increase in temperature. Increase in dielectric constant with increase in temperature in the paraelectric region can also be seen from graphs at 1 kHz frequency that could be related to a low frequency relaxation process. High values of dielectric loss in paraelectric region may be attributed to thermal conductivity losses at elevated temperatures due to the presence of NZF phase. The values of ferroelectric Curie temperature (T_c), room temperature dielectric constant (ε'_{RT}), dielectric constant at T_c (ε'_{max}), room temperature dielectric loss ($\tan\delta_{RT}$) and dielectric loss at T_c for all samples are given in Table 2 for comparison.

Decrease in T_c is observed with increase in Sm substitution which is due to shrinkage in PZT lattice volume and substitution of smaller ionic size Sm^{+3} at Pb site. The values of ε' and $\tan\delta$ given in Table 2 show that Sm substitution results in improved dielectric properties for the given NZF–PSZT composite system.

The typical room temperature variation of dielectric constant (ε') and loss ($\tan\delta$) as function of frequency (10^2–10^6 Hz) is depicted in Fig. 4. It is found that as frequency increases, dielectric constant decreases which accounts for the normal behavior of dielectric materials. Further, if we compare the variation of ε' and $\tan\delta$ with frequency for unsubstituted sample ($x=0$) with that for substituted ones ($x=0.02$ and 0.03), it is observed that the dispersion is decreasing with increase in Sm substitution which can be explained on the basis of the fact that Sm substitution reduces the number of Pb vacancies and counteracts the p-type conduction in PSZT phase resulting in decrease in low-frequency dispersion [12,17]. Similar trends in variation of dielectric properties with frequency are observed for many ferrite-ferroelectric bulk composites [18–20]. NZF–PSZT samples with x=0.02 and 0.03 are suitable for low loss applications in the above given frequency range.

3.3. Ferroelectric properties

To study ferroelectric behavior of NZF–PSZT composite samples, room temperature P–E hysteresis loops were recorded for all the samples and are shown in Fig. 5. P–E loops obtained for all composite samples are unsaturated which may be due to the defects created by the NZF phase because the P–E loops obtained in composites are due to the presence of PSZT as ferroelectric phase and NZF as non-ferroelectric phase. Similar loops were recorded by many research groups [21–23]. It is also observed that the P–E loops are asymmetric about the origin which may be attributed to the internal bias field developed in the ferroelectric phase due to defects [16,24] present in the samples having non-ferroelectric phase. Values of remanant polarization (P_r) and coercive field (E_c) were determined from P–E loops for all the samples and are given in Table 3. With increase in Sm substitution (x), increase in P_r and decrease in E_c was observed except for $x=0.03$. The reason for increase in P_r and decrease in E_c is due to the softening effect of Sm^{+3} resulting in creation of A-site vacancies. It is also well reported in literature that substituents like La and Sm make the materials more soft i.e. increase in P_r and decrease in E_c [25].

3.4. Ferromagnetic properties

To study magnetic behavior of NZF–PSZT composite samples, room temperature M–H hysteresis loops were recorded for all samples and are shown in Fig. 6. All the samples show well defined ferromagnetic behavior and confirm the existence of magnetic ordering in the mixed ferrite-ferroelectric composite system. Values of remanant magnetization (M_r), saturation magnetization (M_s) and coercive field (H_c) were determined from M–H hysteresis loops and are given in Table 3. Small values of H_c for these samples indicate their soft magnetic behavior. Also, with Sm substitution (x), random values of M_r and M_s are observed. This behavior can be understood in terms of the fact that M–H hysteresis loops in NZF–PSZT composites are obtained mainly due to the

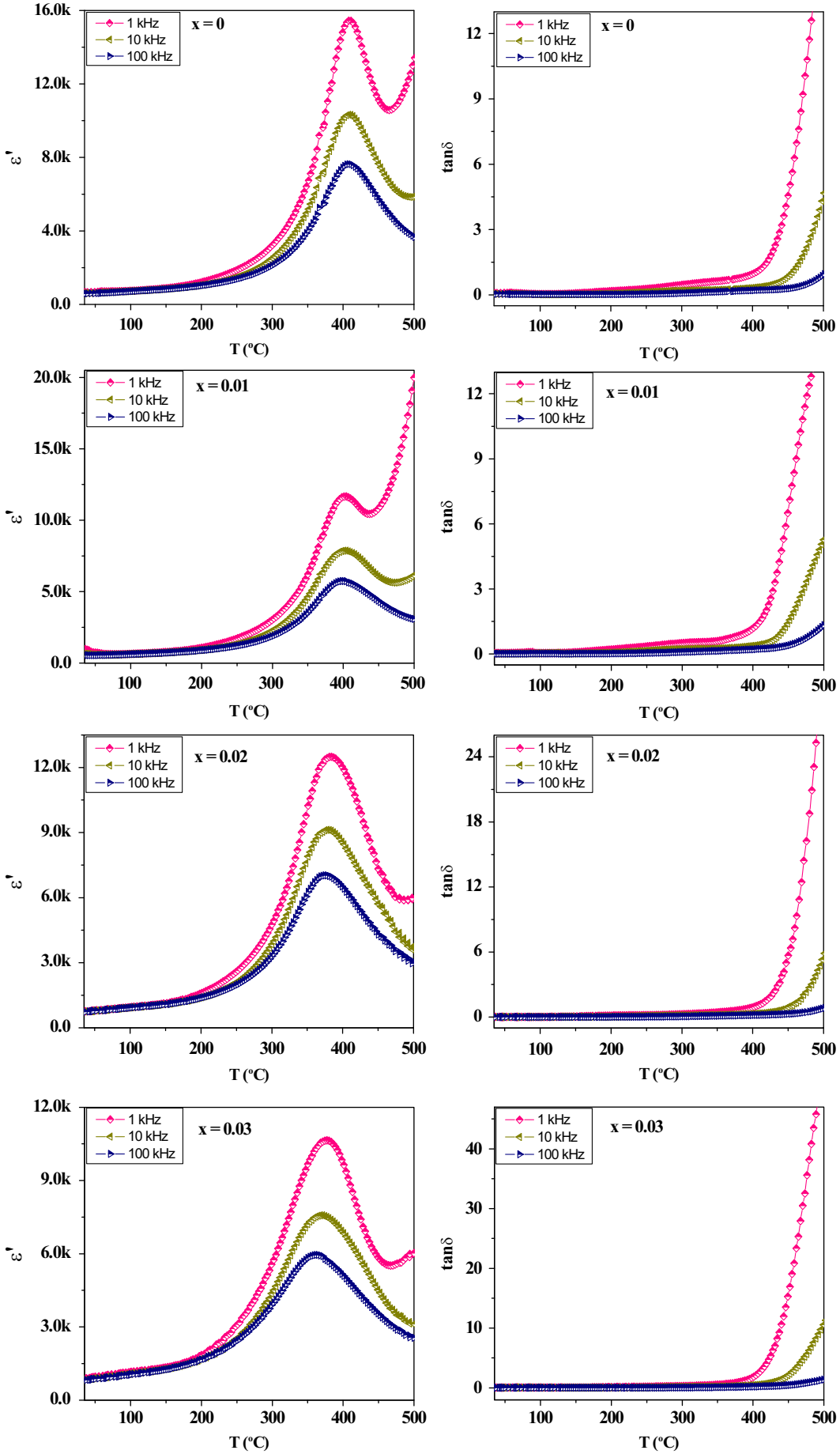

Fig. 3. Variation of dielectric constant (ε') and loss (tan δ) with temperature for NZF–PSZT samples at 1, 10 and 100 kHz.

presence of NZF as magnetic phase while Sm is substituted in ferroelectric phase, PSZT (non-magnetic phase).

3.5. Piezoelectric properties

The values of piezoelectric charge coefficient (d_{33}) for NZF–PSZT composites are listed in Table 3. The d_{33} values are compositional dependent because the composition influences the dielectric permittivity, electrostrictive constant and spontaneous polarization. These parameters are directly related to d_{33} coefficients. As Sm substitution (x) increases from 0 to 0.03, the d_{33} values increases from ~72 pC/N to ~92 pC/N.

3.6. Magnetoelectric properties

Fig. 7 shows the typical variation of ME coupling coefficient (α) with applied DC magnetic field for all samples at room temperature. The appearance of ME signal in NZF–PSZT composites is due to the strain induced in magnetostrictive phase (NZF) by applied magnetic field which leads to polarization in the piezoelectric phase (PSZT). Initially α increases for lower magnetic field values, reaches to maximum and then starts decreasing for higher magnetic field values for all samples. The curves show a maximum at DC magnetic field in the range of ~800–950 Oe.

The maximum value of α is given in Table 3 for all samples. As Sm substitution (x) increases, increase in α is observed which can be attributed to the piezoelectric properties. Sample with $x=0.03$ exhibited the highest ME coupling coefficient due to the fact that its piezoelectric charge coefficient (d_{33}) is higher as compared to other samples. These results are in fair agreement with the theoretical prediction [26]. Maximum α of 22.5 mV/cm Oe is observed for the sample with $x=0.03$ and is higher as compared to those reported for bulk ferrite–ferroelectric composites in literature [27–31].

Table 2
Dielectric parameters for NZF-PSZT samples at 100 kHz.

x	0	0.01	0.02	0.03
T_c (°C)	408	401	375	362
ε'_{RT}	590	550	740	825
ε'_{max}	7635	5740	7025	5950
Tan δ_{RT}	0.03	0.01	0.01	0.02
Tan δ at T_c	0.22	0.21	0.15	0.11

4. Conclusion

NZF–PSZT composites synthesized by the conventional solid state reaction method were characterized by XRD and SEM for structural and microstructural analysis respectively. Sm substitution results in improved dielectric, ferroelectric, piezoelectric and magnetoelectric properties. Observation of both *P–E* hysteresis loops and *M–H* hysteresis loops indicates the presence of ordered ferroelectric and magnetic behavior in the mixed ferrite–ferroelectric composite system. The generation of electric field by applying DC magnetic field is the evidence for magnetoelectric coupling between the constituent phases. The investigated composites showing large ME coupling coefficients seem to be very attractive for applications in multifunctional devices.

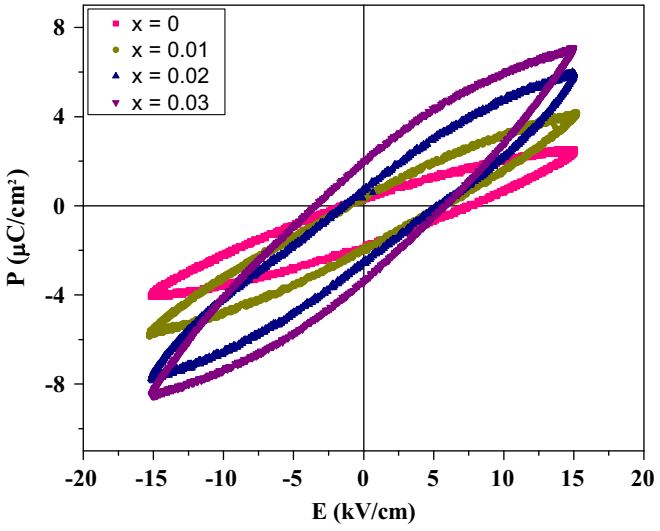

Fig. 5. Room temperature *P–E* hysteresis loops for NZF–PSZT samples at 20 Hz.

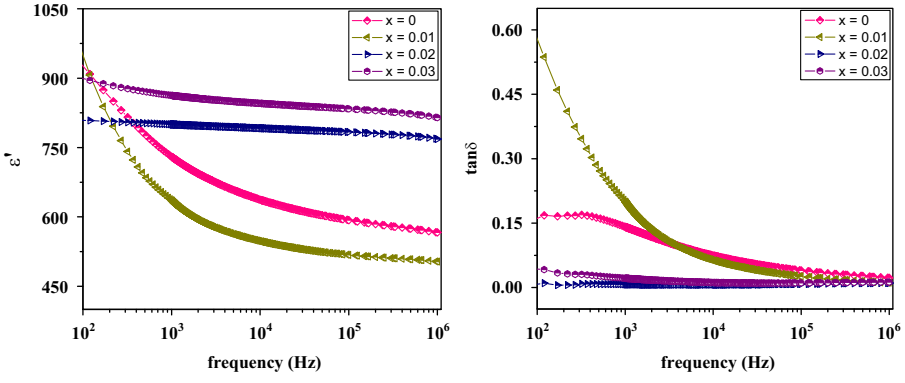

Fig. 4. Variation of dielectric constant (ε') and loss (tan δ) with frequency for NZF–PSZT samples at room temperature.

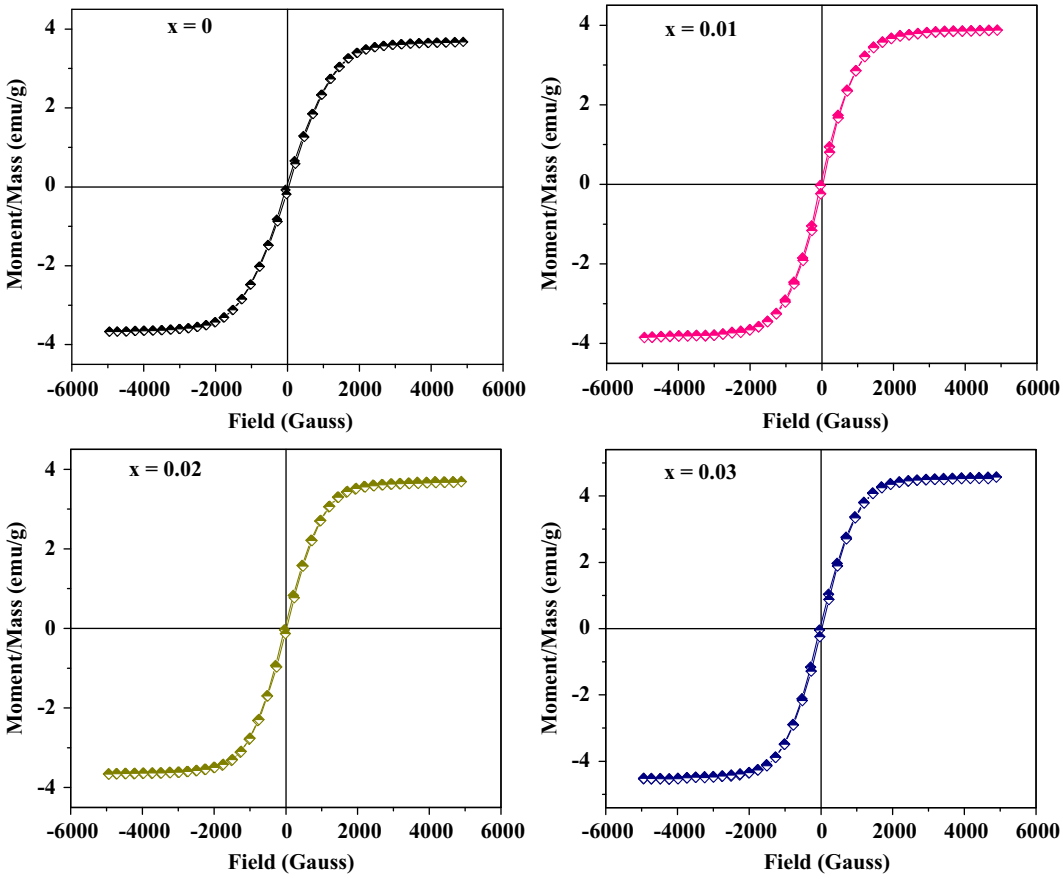

Fig. 6. Room temperature *M–H* hysteresis loops for NZF–PSZT samples.

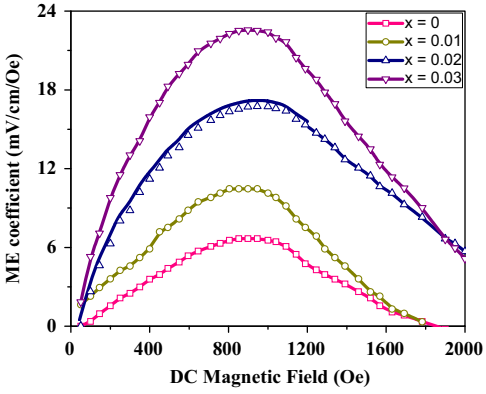

Fig. 7. Variation of ME coupling coefficient (α) with DC magnetic field for NZF–PSZT samples.

Table 3
Ferroelectric, piezoelectric, magnetic and ME parameters for NZF-PSZT samples at room temperature.

Parameters	0	0.01	0.02	0.03
P_r (μC/cm^2)	1.1	1.3	1.7	2.7
E_c (kV/cm)	4.6	3.4	3.3	4.6
M_r (emu/g)	0.09	0.11	0.10	0.12
M_s (emu/g)	3.7	3.9	3.7	4.6
H_c (Gauss)	30	30	30	30
d_{33} (pC/N)	72	75	83	92
α mV/(cm Oe)	6.7	10.5	16.7	22.5

Acknowledgment

One of the authors (Rekha Rani) would like to thank Department of Science and Technology, Government of India for awarding INSPIRE fellowship to her. Authors are thankful to Dr. R.K. Kotnala of National Physical Laboratory, New Delhi for helping in magnetic and magnetoelectric measurements.

References

[1] J.F. Scott, Data storage: multiferroic memories, Nature Materials 6 (2007) 256–257.
[2] M. Gajek, M. Bibes, S. Fusil, K. Bouzehouane, J. Fontcuberta, A. Barthelemy, A. Fert, Tunnel junctions with multiferroic barriers, Nature Materials 6 (2007) 296–302.
[3] M. Vopsaroiu, J. Blackburn, A. Muniz-Piniella, M.G. Cain, Multiferroic magnetic recording read head technology for 1Tb/in2 and beyond, Journal of Applied Physics 103 (2008) 07F506.
[4] S. Dong, J.F. Li, D. Viehland, Vortex magnetic field sensor based on ring-type magnetoelectric laminate, Applied Physics Letters 85 (2004) 2307–2309.
[5] S. Priya, D.J. Inman, Energy harvesting technologies, LLC, 2009.
[6] N. Gupta, A. Verma, S.C. Kashyap, D.C. Dube, Dielectric behavior of spin-deposited nanocrystalline nickel–zinc ferrite thin films processed by citrate-route, Solid State Communications 134 (2005) 689–694.
[7] M.A. Ruiting, Y. Wang, T. Yanwen, Z. Chunli, L. Xikun, Synthesis, characterization and electromagnetic studies on nanocrystalline nickel zinc ferrite by polyacrylamide gel, Journal of Materials Science and Technology 24 (2008) 419–422.

[8] O.P. Thakur, C. Prakash, Structural, dielectric and piezoelectric properties of PLZT (x/60/40) ceramics, Integr, Ferroelectrics 122 (2010) 100–107.
[9] J.K. Juneja, C. Prakash, O.P. Thakur, T.P. Sharma, Dielectric and piezoelectric properties of PZT substituted with samarium, Ferroelectrics Letters 29 (2002) 11–16.
[10] G.H. Haertling, Ferroelectric ceramics history and technology, Journal of the American Ceramic Society 82 (1999) 797–818.
[11] K. Lijima, Y. Tomita, R. Takayama, I. Ueda, Epitaxial growth and crystallographic, dielectric and pyroelectric properties of La modified lead titanate films, Journal of Applied Physics 60 (1986) 2914–2919.
[12] B. Jaffe, W.R. Cook, H. Jaffe, Piezoelectric Ceramics, Academic Press, New York, 1971.
[13] M. Einat, D. Shur, E. Jerby, G. Roseman, Lifetime of ferroelectric Pb(Zr, Ti)O ceramic cathodes with high current density, Journal of Applied Physics 89 (2001) 548–552.
[14] R. Rani, J.K. Juneja, S. Singh, C. Prakash, K.K. Raina, Study of $0.1Ni_{0.8}Zn_{0.2}Fe_2O_4$–$0.9Pb_{1-3x/2}La_xZr_{0.65}Ti_{0.35}O_3$ magnetoelectric composites, Journal of Magnetism and Magnetic Materials 325 (2013) 47–51.
[15] K. Tahmasebi, A. Barzegar, J. Ding, T.S. Herng, A. Huang, S. Shannigrahi, Magnetoelectric effect in $Pb(Zr_{0.95}Ti_{0.05})O_3$ and $CoFe_2O_4$ heteroepitaxial thin film composite, Materials and Design 32 (2011) 2370–2373.
[16] A.S Fawzi, A.D. Sheikh, V.L. Mathe, Multiferroic properties of Ni ferrite-PLZT composites, Physica B: Condensed Matter 405 (2010) 340–344.
[17] J.S. Kim, B.C. Choi, H.K. Yang, J.H. Jeong, Low-frequency dielectric dispersion and electrical conductivity of pure and La-doped $SrBi_2Nb_2O_9$ ceramics, Journal of the Korean Physical Society 52 (2008) 415–420.
[18] L. Zivkovic, B. Stojanovic, C.R. Foschini, V. Paunovic, D. Mancic, Effects of powder preparation and sintering procedure on microstructure and dielectric properties of PLZT ceramics, Science of Sintering 35 (2003) 133–140.
[19] S.B. Narang, D. Kaur, Dielectric anomaly in La modified Barium Titanates, Ferroelectrics Letters 36 (2009) 20–27.
[20] J.Y. Zhai, N. Cai, L. Liu, Y.H. Lin, C.W. Nan, Dielectric behavior and magnetoelectric properties of lead zirconate titanate/Co-ferrite particulate composites, Materials Science and Engineering: B 99 (2003) 329–331.
[21] X. Chao, Z. Yang, M. Dong, Y. Zhang, Piezoelectric, dielectric and magnetic properties of $(1-x)$ Pb[Zr, Ti,$(Mg_{1/2}W_{1/2})$, $(Ni_{1/3}Nb_{2/3})]O_3+x$ (Ni, Co, Cu)FeO_4 composites, Journal of Magnetism and Magnetic Materials 323 (2011) 2012–2016.
[22] D. Pandey, N. Singh, S.K. Mishra, Effect of particle-size on ferroelectric transitions, Indian Journal of Pure and Applied Physics 32 (1994) 616–623.
[23] H.J. Hagemann, Loss mechanism and domain stabilisation in doped $BaTiO_3$, Journal of Physics C 11 (1978) 3333–3345.
[24] A.R. James, J. Subrahmanyam, K.L. Yadav, Structural and electrical properties of nanocrystalline PLZT ceramics synthesized via mechanochemical processing, Smart Materials and Structures 39 (2006) 2259–2263.
[25] J.D. Mackenzie, Y. Xu, Ferroelectric materials by the sol–gel method, Journal of Sol-Gel Science and Technology 8 (1997) 673–679.
[26] C.W. Nan, Magnetoelectric effect in composites of piezoelectric and piezomagnetic phases, Physical Review B 50 (1994) 6082–6088.
[27] D.R. Patil, S.A. Lokare, R.S. Devan, S.S. Chougule, Y.D. Kolekar, B. K. Chougule, Dielectric properties and magnetoelectric effect of (x) $NiFe_2O_4+(1-x)$ $Ba_{0.8}Sr_{0.2}TiO_3$ composites, Journal of Physics and Chemistry of Solids 68 (2007) 1522–1526.
[28] C.M. Kanamadi, J.S. Kim, H.K. Yang, B.K. Moon, B.C. Choi, J.H. Jeong, Magnetoelectric effect and complex impedance analysis of $(x)CoFe_2O_4+(1-x)Ba_{0.8}Sr_{0.2}TiO_3$ multiferroics, Journal of Alloys and Compounds 481 (2009) 781–785.
[29] A. Gupta, R. Chatterjee, Study of dielectric and magnetic properties of $PbZr_{0.52}Ti_{0.48}O_3$–$Mn_{0.3}Co_{0.6}Zn_{0.4}Fe_{1.7}O_4$ composite, Journal of Magnetism and Magnetic Materials 322 (2010) 1020–1025.
[30] V.M. Laletin, V.M. Petrov, Nonlinear magnetoelectric response of a bulk magnetostrictive–piezoelectric composite, Solid State Communications 151 (2011) 1806–1809.
[31] A.D. Sheikh, V.L. Mathe, Dielectric, ferroelectric, magnetic and magnetoelectric properties of PMN-PT based ME composites, Journal of Physics and Chemistry of Solids 72 (2011) 1423–1429.